Thin Solid Films 669 (2019) 345–350

Contents lists available at ScienceDirect

Thin Solid Films

journal homepage: www.elsevier.com/locate/tsf

Device simulation of $Cu(In,Ga)Se_2$ solar cells by means of voltage dependent admittance spectroscopy

Torsten Hölscher[a,*], Thomas Walter[b], Thomas Schneider[a], Matthias Maiberg[a], Roland Scheer[a]

[a] Martin-Luther-University Halle-Wittenberg, Von-Danckelmann-Platz 3, 06120 Halle (Saale), Germany
[b] University of Applied Sciences Ulm, Albert-Einstein-Allee 55, 89081 Ulm, Germany

ARTICLE INFO

Keywords:
Thin film solar cells
Copper indium gallium diselenide
Admittance spectroscopy
Device simulation
Interface recombination
Deep defects

ABSTRACT

The simulation of solar cell devices is important for the understanding of defect physics and loss mechanisms in real solar cells. On the other hand, voltage dependent admittance spectroscopy delivers essential information for establishing a baseline simulation model of $Cu(In,Ga)Se_2$ (CIGSe) solar cells. Here we give an explanation for the weak temperature dependence of the N1-signal, the latter being not compatible with a bulk defect or with a simple hole barrier at the Mo back contact. Furthermore, we find a $E_{d,IF} - E_V \approx 0.3$ eV deep recombination-active acceptor state at the absorber/buffer interface made of air-light exposed CIGSe absorbers. This gives us the ability to explain the reduction of power conversion efficiency of solar cells made from air-light exposed absorbers. From the voltage dependent capacitance step of this interface defect we can deduce the formerly unknown position of the Fermi level at the hetero junction in equilibrium which is close to mid-gap. Simulation of dark J-V curves allows a refinement of the parameter of this absorber/buffer interface defect, resulting in a defect density of $N_{d,IF} \approx 3.5 \cdot 10^{11}\,cm^{-2}$ as well as capture cross sections of $\sigma_n \approx 4 \cdot 10^{-16}\,cm^2$ for electrons and $\sigma_p \approx 3 \cdot 10^{-11}\,cm^2$ for holes.

1. Introduction

Since long the development of $Cu(In,Ga)Se_2$ (CIGSe) solar cells is escorted by a variety of characterization methods [1]. However, a lot of material parameters such as defect densities or dominant regions of recombination influencing the electronic properties of the CIGSe layer are still obscured, albeit being of large interest [1–3]. Admittance spectroscopy is a common method to monitor chargeable defects within the bandgap [4–6]. The analysis of admittance signatures gives information about the defect properties like density of states, energy levels, and capture cross sections [7,8]. An often observed feature is a capacitance step with activation energies in the range of 50. 150 meV and formerly baptised as N1 [7–9]. Applying a DC bias voltage during admittance measurements allows the distinction between a spatial narrow and an extended defect such as interface and bulk defects. In most cases the N1 signal shows no reaction to a DC bias voltage [4,6,8,10]. Without Fermi level pinning this behaviour is dedicated to a bulk defect or explained by a transport barrier for charge carriers [9,11–13]. However, in this work we show by 1-dimensional device simulation using *SCAPS 1d* that a bulk defect or a charge carrier barrier do not describe the weak temperature dependence of the N1 signal as observed in the experimental data. Further, we can explain by virtue of a deep acceptor like interface defect the additional voltage dependent signature in admittance spectroscopy of solar cells with air-light exposed (ALE) CIGSe layers (see our former study [10]). Concatenation with dark J-V curves reduces the space of free parameters such as capture cross sections or the defect density for this interface state. We show that the shape of our capacitance-frequency (C-f) curves is influenced by both deep acceptor and donor bulk defects in the CIGSe absorber layer. Finally, we present a baseline model of our solar cell devices.

2. Experimental

The CIGSe absorbers layers of the investigated solar cells were grown by a 3-stage co-evaporation process. As substrates served molybdenum covered soda lime glass (SLG). During the 2. and 3. stage of the CIGSe growth process, Na was incorporated by diffusing from the SLG into the CIGSe layer at a substrate temperature of 625 °C. The integral elemental ratios of the final CIGSe layers were determined with energy dispersive X-ray diffraction to [Cu]/([Ga] + [In]) ≈ 0.90 and [Ga]/([Ga] + [In]) ≈ 0.28, respectively.

For this study, we compare 2 samples, CIGSe A and B, differing in their ALE status of the CIGSe absorber layer. The bare CIGSe absorber of

* Corresponding author.
E-mail address: torsten.hoelscher@physik.uni-halle.de (T. Hölscher).

https://doi.org/10.1016/j.tsf.2018.11.022
Received 13 July 2018; Received in revised form 7 November 2018; Accepted 12 November 2018
Available online 14 November 2018
0040-6090/

sample CIGSe A received a 60 min ALE-treatment with 1 sun equivalent white light from a 3350 K tungsten halogen lamp in air and at room temperature. Sample CIGSe B served as reference and stayed for 60 min in ambient air but without illumination. More details are given in Ref. [2, 10].

Immediately after the ALE experiment, the CdS buffer layer (≈50 nm) was processed on to the CIGSe layers by chemical bath deposition. The solar cells were completed by sputtering 50 nm non-doped and 350 nm Aluminium doped ZnO layers. For electrical characterization a Ni/Al/Ni metal grid was evaporated on top of the layer stack. Three solar cells (0.5 × 1 cm^2) per substrate (2 × 2 cm^2) were defined by mechanical scribing. After measuring dark and illuminated J-V curves the cell size was reduced to ≈0.2 cm^2 likewise with mechanical scribing, with the intention to reduce the series resistance in admittance spectroscopy.

Before cooling down to 90 K the samples were relaxed for > 10 h at 300 K and in darkness. During admittance spectroscopy, the temperature was varied in 10 K steps from 90 to 300 K and measured with a *CY7 Omega* Si-diode mounted directly on the sample surface. The C-f analysis was conducted with an *Agilent E4980A* LCR meter from 100 to 10^6 Hz and an AC signal amplitude of 50 mV. A DC bias voltage was applied in the range from −1 to 0.75 V. In this contribution, we restrict ourselves to temperatures between 110 K and 300 K as well as to bias voltages between −0.5 V and + 0.375 V.

3. Results

Dark and illuminated J-V curves of sample CIGSe A (60 min ALE) and CIGSe B (No ALE) are presented in Fig. 1. Both samples reveal a similar short circuit current density J_{SC} of ≈33 mA·cm^{-2} whereas open circuit voltage V_{OC} and fill factor FF of the 60 min treated ALE sample are reduced by ≈10% with respect to the non-ALE sample. Hence the efficiency η declines from ≈17% to ≈14% by the ALE treatment. Further, the dark and illuminated J-V curves of sample CIGSe A exhibit a cross over (marked by the black circle) implying a high density of acceptor states at the CIGSe/CdS interface (see Section 7.1.2 in Ref. [14]).

The experimental admittance data of the 60 min ALE treated sample CIGSe A are shown on the left hand sided column (a)–(e) of Fig. 2. The applied DC bias voltage is indicated by the text box in the top right corner of each plot. On the right hand sided column (f)–(j), the calculated expression $-\omega \cdot dC/d\omega$ of the measured C-f curves for particular temperature ranges is displayed. Generally, a capacitance step in the C-f spectra, e.g. as provoked by a defect state, generates a peak in this display form of the data. The peak maximum frequency equals the inflection point ω_0 of the capacitance step and thus the escape frequency of the defect level [7,8]. An advantage of this display form is that defect signatures can be determined more reliably even in the case of overlapping or weak steps in the C-f curves.

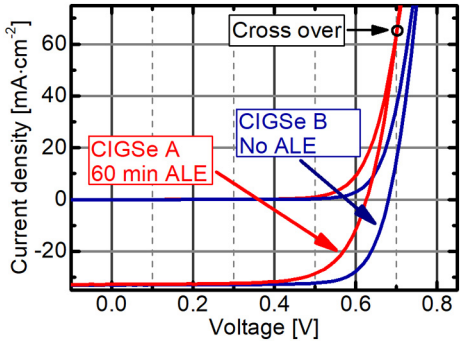

Fig. 1. Dark and illuminated J-V curves of solar cells consisting of the 60 min ALE treated absorber CIGSe A and the non-ALE absorber CIGSe B. With V_{OC} = 626 mV, J_{SC} = 32.8 mA, FF = 70.0% and η = 14.3% for CIGSe A as well as V_{OC} = 681 mV, J_{SC} = 33.0 mA, FF = 77.1% and η = 17.3% for CIGSe B.

It is apparent from Fig. 2(g), (h), and (i) that under a forward bias a voltage dependent admittance signature – named IF (interface) in Fig. 2 – becomes visible: For the 0 V and 0.125 V biased measurements a temperature dependent broad peak with a high (IF_{high}) and a low (IF_{low}) frequency flank is existent in Fig. 2(g) and (h). The low frequency flank shifts to higher frequencies. The high frequency flank of the IF feature (IF_{high}) disappears with increasing bias voltage due to increasing overlap with the N1 signature (see Fig. 2i–j). Thus, indeed the peak-position of the IF feature is shifting to higher frequencies with increasing bias voltage. This means that the activation energy of the IF defect signature is voltage dependent with a smaller energy at larger voltage. This behaviour is typical for a spatially narrow and energetically broad defect state like in the case of an interface defect [14].

At low frequencies ($\omega \approx 10^3\ s^{-1}$) a further signal – named as B in Fig. 2 – becomes visible. The appearance at high temperature (T ≈ 300 K) and the bias voltage independence of this feature points towards a deep bulk defect. The shape of the C-f curves at high temperatures (T ≈ 300 K) at the point S in Fig. 2(b)–(e), we assign to an overlap of the B and IF signatures. The signal curve in Fig. 2(g) at 300 K confirms this assumption, where only the B and IF peak flanks are visible. In the case of the B signal the $-\omega \cdot dC/d\omega$ expression implicates a peak maximum at $\omega \approx 800\ s^{-1}$ resulting from the uncertainty of the derivative in the first frequency points indicated by the red rectangles in Fig. 2(f)-(j). A measurement artefact of increasing capacitance exists for high frequencies and temperatures above 230 K, indicated by the dashed line and the arrow in Fig. 2(a).

4. Device simulation

4.1. Default model

Fig. 3(a) shows the equilibrium band diagram of our starting device at 300 K which is the default device. This model is based on our former study with time-resolved photoluminescence (TRPL) and 1d simulations by *TCAD® Sentaurus* [15]. There we found an electron trap D2 close to the conduction band E_C. Next, the Shockley-Read-Hall lifetime for electrons and for holes was determined to $\tau_n \approx 10$ ns and to $\tau_p \approx 2000$ ns, respectively [15]. To this end, we introduced a discrete deep donor type defect D1 at midgap and adjusted the capture cross sections to the measured lifetimes. Table 1 lists the electrical and defect properties of the CIGSe absorber layer. The properties of the window layers are not within the scope of this work and are adopt from Table 8.4 of Ref. [14] with minimal modified doping concentrations in the case of the non-doped ZnO and the Aluminium doped ZnO.

For the temperature dependence of the parameters in Table 1 we assumed $N_{C,V} \propto (T/T_0)^{3/2}$ for the effective density of states, $v_{n,p}^{th} \propto (T/T_0)^{1/2}$ for the thermal velocities, and $\mu_p \propto (T/T_0)^{-3/2}$ for the hole mobility of the CIGSe absorber layer, with T_0 = 300 K. This gives a hole mobility of $\mu_p \approx 45\ cm^2 \cdot V^{-1} \cdot s^{-1}$ at T = 110 K employing $\mu_p = 10\ cm^2 \cdot V^{-1} \cdot s^{-1}$ at 300 K, the latter being close to the measurement value in Ref [16]. The temperature dependence of all other parameters in Table 1 revealed a negligible influence to the admittance simulations. With this, and in order to keep the complexity of our simulation model small, we excluded the temperature dependence of μ_n, σ_n, σ_p, and E_g .

Fig. 3(b) shows the simulated C-f curves of the default device with 0 V biased voltage. The shape of the C-f curves at low temperatures originates from the tail like acceptor defect A1 and represents the transition to the geometrical device capacitance C_{geo} at higher frequencies. No further pronounced feature can be seen in this admittance spectrum although the Fermi level E_F is crossing the D1 level, as indicated by the yellow circle in Fig. 3(a). As the density of defect D1 with $10^{-13}\ cm^{-3}$ is very small, this defect contributes only weakly to the junction capacitance.

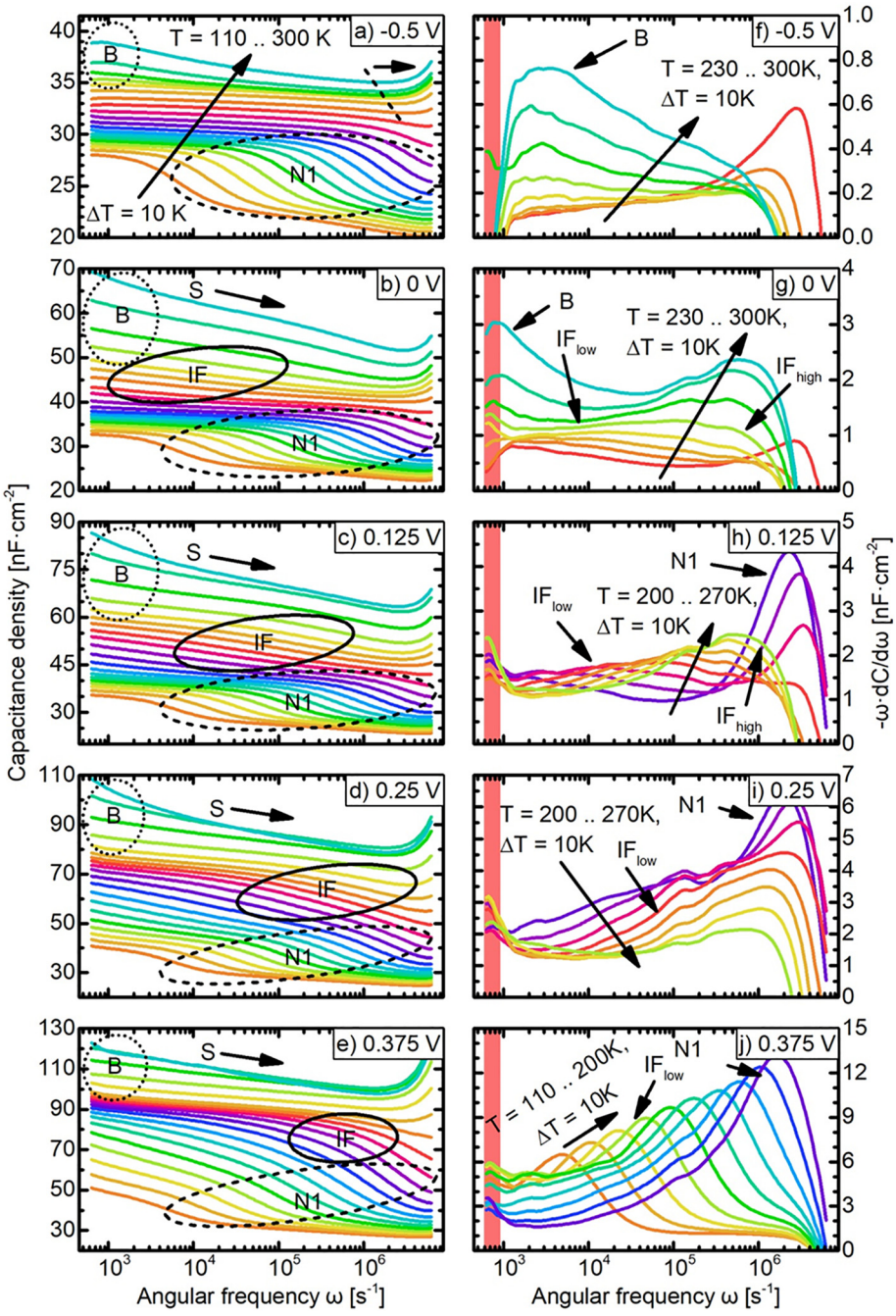

Fig. 2. (a)-(e): Admittance spectra of the 60 min ALE treated sample CIGSe A measured under a varied DC bias voltage from −0.5 V to +0.375 V. The measurement temperature was adjusted in the range from 110 K to 300 K in 10 K steps. Remarkable features B, IF, and N1 are highlighted by ellipses. The shape of the capacitance curves is indicated by an arrow and the letter S. (f)-(j) Visualization of the signatures B, IF, and N1 with the expression $-\omega \cdot dC/d\omega$ in the given temperature range.

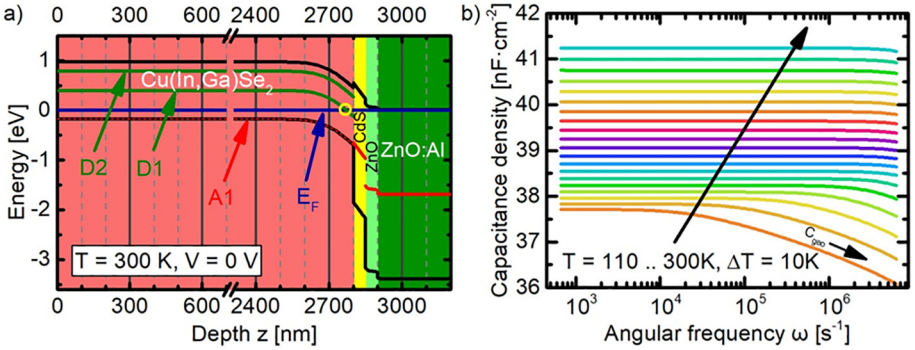

Fig. 3. (a) Equilibrium band diagram of the default simulation model. The band edges are coloured in black, acceptor like defects are coloured in red, and donor like defects are coloured in green. The yellow circle marks the crossing point of the Fermi level E_F with the donor defect D1. (b) Simulated C-f curves of the device in (a). (For interpretation of the references to colour in this figure legend, the reader is referred to the web version of this article.)

Table 1
Electronic and defect properties of the CIGSe absorber layer for the default simulation device at $T = 300$ K. With d thickness, χ_e electron affinity, E_g band gap energy, ε_r specific permittivity, $N_{C,V}$ effective density states of the conduction and valence band, $v_{n,\ p}{}^{th}$ thermal velocity, and $\mu_{n,p}$ mobility for electrons and holes. N_A is the constant p-type doping concentration of the absorber layer. The defect properties are given with N_d defect density, E_d energy level, $\sigma(E_d)$ energetically defect distribution, $\sigma_{n,p}$ capture cross section, and $(\sigma_{n,p}{\cdot}v_{n,\ p}{}^{th}{\cdot}N_d)^{-1}$ capture time of electrons and holes. The energetically defect distributions are declared by (g) for Gaussian and (t) for Tail like distributions.

Properties	CIGSe absorber
d [μm]	2.8
χ_e [eV]	4.5
E_g [eV]	1.15
ε_r	13.6
N_C [cm^{-3}]	$7{\cdot}10^{17}$
N_V [cm^{-3}]	$1.5{\cdot}10^{19}$
$v_{n,\ p}{}^{th}$ [$cm{\cdot}s^{-1}$]	10^7
$\mu_{n,p}$ [$cm^2{\cdot}V^{-1}{\cdot}s^{-1}$]	10
N_A [cm^{-3}]	$7{\cdot}10^{15}$

Defects	D1	D2	A1
N_d [cm^{-3}]	10^{13}	$1.5{\cdot}10^{16}$	$2.5{\cdot}10^{16}$
$E_d - E_V$ [eV]	Midgap	0.965	0
$\sigma(E_d)$ [eV]	discret	0.035 (g)	0.08 (t)
σ_n [cm^2]	10^{-12}	$2{\cdot}10^{-13}$	10^{-17}
σ_p [cm^2]	$5{\cdot}10^{-15}$	10^{-17}	10^{-14}
$(\sigma_n{\cdot}v_n{}^{th}{\cdot}N_d)^{-1}$ [ns]	10	0.05	400
$(\sigma_p{\cdot}v_p{}^{th}{\cdot}N_d)^{-1}$ [ns]	2000	910	0.4

4.2. N1-Signature

In this section we want to introduce the N1 capacitance step in our simulations. As shown in Fig. 2, the N1 feature is independent from the applied bias voltage. An Arrhenius plot (not shown) of the quantity ln $(\omega_0 T^{-2})$ reveals an activation energy of $E_a \approx 0.1$ eV. In line with this and with the energetic position of the Fermi-level in Fig. 3(a), a shallow acceptor like bulk defect or a majority charge carrier transport barrier at the back contact (BC) could be responsible for the N1 signal. With the thermionic emission theory the characteristic frequency ω_0 of a transport barrier is given in Eq. (1) [14].

$$\omega_0 \propto A^* \cdot T^2 \cdot exp\left\{-\frac{\Phi_B}{kT}\right\} \tag{1}$$

Here A^* denotes the effective Richardson constant and k the Boltzmann constant. Obviously ω_0 and the temperature dependence of ω_0 depends on both Φ_B and A^*, where $A^* \propto m_p{}^*$ is linked to $N_V \propto (m_p{}^*)^{3/2}$ via the effective hole mass $m_p{}^*$. As compared to $A^* \approx 120$ $A{\cdot}cm^{-2}{\cdot}K^{-2}$ for the free electron mass, using the value for $N_V = 1.5{\cdot}10^{19}$ cm^{-3} in Table 1, we can estimate $A^* \approx 85$ $A{\cdot}cm^{-2}{\cdot}K^{-2}$.

Fig. 4(a)-(c) shows 3 scenarios for a transport barrier at 110 K. In the first case, Fig. 4(a), we introduced a Schottky barrier at the back contact. On the one hand to yield the experimental characteristic frequency $\omega_0 \approx 6000\ s^{-1}$ at $T = 110$ K the metal workfunction has been fixed to $\Phi_m = 5.42$ eV. This results in a barrier height of $\Phi_B = 0.23$ eV which is in a strong contrast to the experimental determined activation energy of 0.1 eV. On the other hand to achieve $\omega_0 \approx 6000\ s^{-1}$ with a barrier height $\Phi_B = 0.1$ eV a reduction of A^* by $\approx 10^3$ is necessary, resulting in a reduction of N_V from 10^{19} cm^{-3} to 10^{14} … 10^{15} cm^{-3}. With such low effective density of states, the absorber becomes electronically degenerate. This is why henceforth we focus on a Schottky barrier height with 0.23 eV. As seen in Fig. 4(d), the temperature dependence of ω_0 for this barrier height is much stronger than that of the experimental data. This could be explained by a shift of the Fermi-level into the band gap with increasing temperature due to the temperature dependence of N_V – and thus by a reduced band bending. In order to overcome this problem, a type of barrier is needed which counteracts the reduction of band bending. In Fig. 4(b), we inserted a barrier in the form of a grain boundary with a CIGSe/CIGSe interface (IF) and with donor like interface states ($N_t \approx 4{\cdot}10^{11}$ cm^{-2}). The parameters of the interface states were deliberately adopted from the D2 defect in Table 1 although similar defect parameters could be used for simulation with identical results. In Fig. 4 (d) the slope of ω_0 as a function of temperature for this Bulk Barrier is smaller than that of the Schottky Barrier, but is still far from the experimental data. A further reduction of the ω_0(T)-slope can be achieved by lowering the p-type doping of the CIGSe absorber, however in that case the experimental capacitance of $C \approx 30$ $nF{\cdot}cm^{-2}$ especially at low temperatures and low frequencies (see Fig. 2) cannot be reproduced by simulation.

Another approach is shown in Fig. 4(c). Here we inserted a 30 nm n-type interfacial layer (IL) between the metal back contact and the CIGSe absorber. The metal work function was fixed to $\Phi_m = 5.5$ eV, which gives a nearly flatband condition at 110 K and an ohmic contact at 300 K. A constant n-type doping of $N_D = 10^{15}$ cm^{-3} to the IL was applied, the band gap was set to the CIGS band gap of $E_g = 1.15$ eV. The defects D2, A1 were removed in the IL and D1 was inverted to an acceptor like defect state. This newly formed second diode would not create a capacitance step like the N1 signal itself (compare the band bending in Fig. 4(a) and (c)), because of the screening effect of the metal contact. Hence, the thermionic emission over this barrier has to be reduced. Again, this can be achieved by reducing N_V ($\approx 10^{16}$ cm^{-3}) of the interfacial layer, which means a decreased $m_p{}^*$ and thus a reduced effective Richardson constant as shown in Ref. [17] for GaAs. The temperature dependence of ω_0 in Fig. 4(d) for this interfacial barrier fits best to the experimental data.

For the sake of completeness, we mention that a bulk defect with $E_d = E_a = 0.1$ eV does not intersect the Fermi-level. On the other hand a deeper defect, crossing the Fermi-level becomes possible by increasing the hole capture cross section σ_p as seen in Eq. (2) after Ref. [8].

$$\omega_0 \propto \sigma_p \cdot exp\left\{-\frac{E_a}{kT}\right\} \tag{2}$$

Analogous, an increased σ_p causes an higher activation energy and

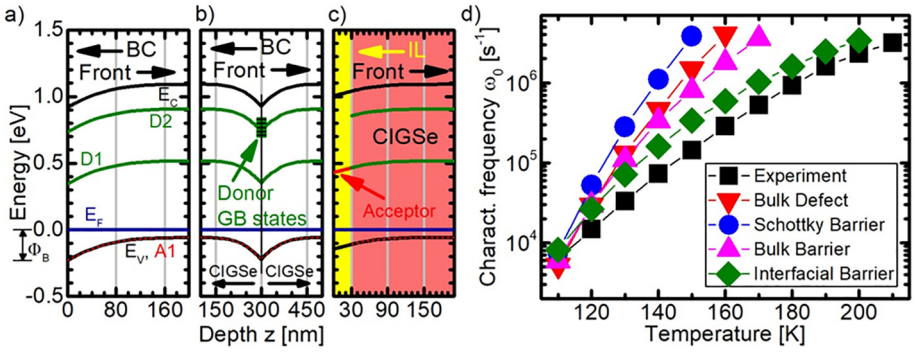

Fig. 4. (a)-(c) Simulated equilibrium band diagrams of different majority charge carrier barriers at a temperature of 110 K. With (a) a Schottky barrier due to the work function of the metal back contact, (b) a barrier induced by a positive charged interface within the bulk, and (c) with an n-type interfacial layer (IL) between the CIGSe absorber and the back contact metalization. (d) The characteristic frequency ω_0 as a function of temperature for the respective N1 scenario capacitance step.

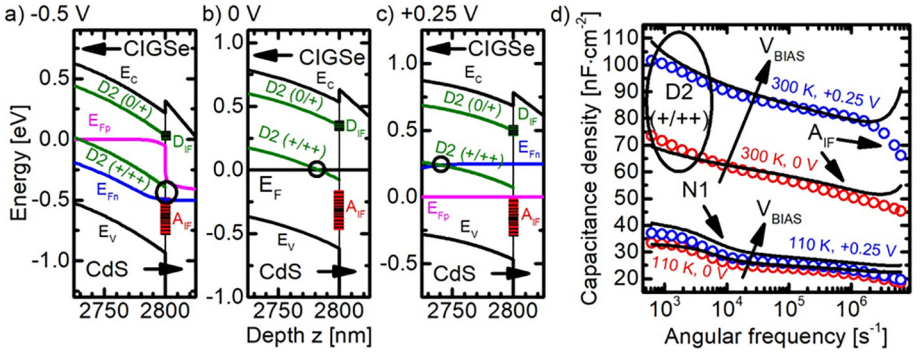

Fig. 5. (a)-(c) Simulated band diagrams at the CIGSe/CdS interface under different applied bias voltages. Donor states are coloured in green and acceptor states are coloured in red. (d) Experimental (black solid lines) and simulated (circles) C-f curves of the 60 min ALE treated sample CIGSe A for 110 K and 300 K as well as 0 V (red) and 0.25 V (blue) biased voltage. (For interpretation of the references to colour in this figure legend, the reader is referred to the web version of this article.)

therefore a stronger temperature dependence of the characteristic frequency. To reproduce the experimental $\omega_0(110K)$ a simulated bulk defect ($N_d \approx 10^{16}\,cm^{-3}$) with $\sigma_p = 10^{-14}\,cm^2$ yields an energy level of E_d- $E_V = 0.18$ eV which indeed crosses the Fermi-level. As shown in Fig. 4(d), due to the too strong temperature dependence of ω_0 this bulk defect also cannot be responsible for the N1-signal. Thus at the current status, an n-type IL layer is the most suitable explanation for the often observed weak temperature dependence of the N1 signature [6,12,18–20].

4.3. Bulk and interface defects

Applying a DC bias voltage not only gives us the possibility to distinguish between a spatially narrow and a spatially extended defect, but also gives us an indication on the energy level as well as on the defect distribution and defect type (donor/acceptor). We want to start with the signature B shown in Fig. 2 and dedicate it to a deep bulk defect. The hole quasi Fermi-level E_{Fp} in Fig. 5 (a) and (c) does not cross the defect level anymore wherefore an acceptor state can be ruled out. Thus, with Fig. 5 (a)-(c) we can show that this signature deals with a donor type defect being located at a level below midgap with $E_C - E_d = 0.61$ eV. The simulations for such a deep donor state reveal a defect density of $N_d \approx 10^{16}\,cm^{-3}$, which is in the range of the D2 electron trap found by TRPL. Without restriction of the generality we tend to assign this defect to the second (+/++) ionisation transition of the D2 state, named as D2 (+/++). Certainly, admittance signature B could also be due to another defect with coincidently equal concentration as D2. If we assign the midgap defect to D2 (+/++) all defect parameters except for $E_C - E_d = 0.61$ eV, $\sigma_n = 10^{-11}\,cm^2$, and $\sigma_p = 10^{-19}\,cm^2$ are given in Table 1 by the description of defect D2. These cross sections have been selected in order match the admittance measurement (σ_n) and in order to avoid strong recombination (σ_p). The large electron and small hole capture cross sections are in agreement with a (+/++) transition level.

In Fig. 5 (a), the electron quasi Fermi-level E_{Fn} almost reaches the D2 (+/++) level at the CIGSe/CdS interface. This would cause a weak signal in the admittance spectrum because only the flank of the Gaussian distributed defect contributes to the capacitance step. This can indeed be observed at low frequencies for the B feature in Fig. 2 (a). For higher bias voltages (> -0.5 V) the capacitance step vanishes and the capacitance at low frequencies does not saturate due to the complete crossing of the electron quasi Fermi- and defect level. For a better overview we do not display the D1 and A1 levels in Fig. 5.

To simulate the IF signature in Fig. 2 we tested a donor like (D_{IF}) as well as an acceptor like (A_{IF}) defect state at the CIGSe/CdS interface. It can be seen from Fig. 5 (a)-(c) that the distance between E_{Fn} and E_C is changing weakly under modified bias voltages. In contrast, E_{Fp} - E_V shows a high receptiveness to voltage changes. Therefore the shifting character of the IF signature in Fig. 2 is better explained by an acceptor like defect state A_{IF} at the interface. Further we find that the strong increase of the capacitance with increasing forward bias (see arrow V_{BIAS} in Fig. 5d) can be referred to an voltage enhanced contribution of A_{IF} to the junction capacitance. This strong capacitance increase cannot be explained by the diffusion capacitance. However, in order to simulate the large V_{BIAS} effect, we need a high density of A_{IF}. The simulated C-f curves in Fig. 5 (d) reveals for the A_{IF} defect state a hole capture cross section of $\sigma_p = 3{\cdot}10^{-11}\,cm^2$, an energy level of $E_d = 0.3$ eV with a Gaussian distribution of $\sigma(E_d) = 0.15$ eV, and a density of $N_d = 3.5{\cdot}10^{11}\,cm^{-2}$.

Although A_{IF} can explain the IF admittance signature, we are forced to introduce an interface donor state D_{IF}. This is due to the requirement that without ALE (small A_{IF} density for sample CIGSe B) the position of the equilibrium Fermi level migrates to a higher level within the bandgap. Thus E_{Fp} (under bias voltage) does no longer intersect A_{IF} and hence no IF signature is detectable in admittance spectroscopy (see Ref. [10]).

4.4. J-V curves

To determine the electron capture cross section σ_n of the A_{IF} defect state the simulation of dark J-V curves was used. Fig. 6 shows simulated and measured J-V curves of the 60 min ALE treated sample CIGSe A and the non-ALE sample CIGSe B. From the simulations we can deduce $\sigma_n \approx 4{\cdot}10^{-16}\,cm^2$ for the electron capture cross section in the case of sample CIGSe A. By reducing N_d to $\leq 3{\cdot}10^{10}\,cm^{-2}$ the J-V curves of sample CIGSe B are well described.

5. Conclusion

To summarize, we are able to show that the simulation of voltage dependent admittance measurements gives a plethora of information about the defect physics of the CIGSe absorber layer. We find a deep donor like bulk defect with E_C - $E_d = 0.61$ eV. The temperature dependence of the characteristic frequency of the N1 signal was simulated by means of several models. Based on our simulations we are able to

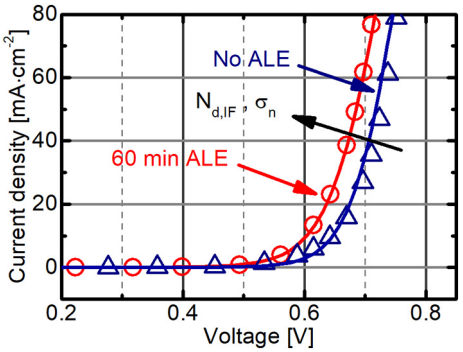

Fig. 6. Simulated (symbols) as well as experimental (solid lines) dark J-V curves of sample CIGSe A with a 60 min ALE treated CIGSe absorber and of sample CIGSe B with a non-ALE treated absorber.

exclude a shallow acceptor like bulk defect as well as a conventional Schottky barrier at the back contact. A good approximation of the experimental N1 signal points towards an n-type interfacial layer with reduced N_V ($\approx 10^{16}\,cm^{-3}$) at the metal back contact. Regarding the voltage dependent IF signal in admittance measurements of solar cells with ALE treated absorber layers the simulation data reveal a recombination-active acceptor like interface state A_{IF}. We are able to determine the characteristic parameter of A_{IF} with $E_d = 0.3\,eV$, $\sigma_p = 3{\cdot}10^{-11}\,cm^2$, and $N_d = 3.5{\cdot}10^{11}\,cm^{-2}$ from simulations of voltage dependent admittance spectroscopy. The remaining parameter $\sigma_n = 4{\cdot}10^{-16}\,cm^2$ can be deduced by simulation of the respective dark J-V curves. Reducing the defect density by 1 order of magnitude of the interface defects well describes the superior cell parameter of devices with non-ALE absorber layers.

Acknowledgements

This work was funded by the Deutsche Forschungsgemeinschaft (DFG) under project SCHE 1745/4-1. The authors thank sincerely the *ROGERS CORPORATION* for providing us with RT/duroid®6002 laminates to realize the electrical connection under cryogenic conditions of our samples.

References

[1] D. Abou-Ras, M. Bär, R. Caballero, R. Gunder, C. Hages, M.D. Heinemann, C.A. Kaufmann, M. Krause, S. Levcenco, R. Mainz, J. Marquez, A. Nikolaeva, A. Redinger, N. Schäfer, S. Schorr, H. Stange, T. Unold, R.G. Wilks, Advanced characterization and in-situ growth monitoring of Cu(In,Ga)Se_2 thin films and solar cells, Sol. Energy 170 (2018) 102–112.

[2] T. Hölscher, S. Förster, T. Schneider, M. Maiberg, W. Widdra, R. Scheer, Light induced degradation of Cu(In,Ga)Se_2 thin film surfaces, Appl. Phys. Lett. 111 (2017) 011604.

[3] J. Chantana, T. Kato, H. Sugimoto, T. Minemoto, Heterointerface recombination of Cu(In,Ga)(S,Se)$_2$-based solar cells with different buffer layers, Prog. Photovolt. Res. Appl. 26 (2018) 127–134.

[4] T.P. Weiss, S. Nishiwaki, B. Bissig, S. Buecheler, A.N. Tiwari, Voltage dependent admittance spectroscopy for the detection of near interface defect states for thin film solar cells, Phys. Chem. Chem. Phys. 19 (2017) 30410–30417.

[5] S.J. Heise, V. Gerliz, M.S. Hammer, J. Ohland, J. Keller, I. Hammer-Riedel, Light-induced changes in the minority carrier diffusion length of Cu(In,Ga)Se_2 absorber material, Sol. Energy Mater. Sol. Cells 163 (2017) 270–276.

[6] F. Werner, S. Siebentritt, Buffer layers, defects, and the capacitance step in the admittance spectrum of a thin-film solar cell, Phys. Rev. Appl. 9 (2018) 054047.

[7] T. Walter, R. Herberholz, C. Müller, H.W. Schock, Determination of defect distributions from admittance measurements and application to Cu(In,Ga)Se_2 based heterojunctions, J. Appl. Phys. 80 (8) (1996) 4411–4420.

[8] R. Herberholz, M. Igalson, H.W. Schock, Distinction between bulk and interface states in $CuInSe_2$/CdS/ZnO by space charge spectroscopy, J. Appl. Phys. 83 (1) (1998) 318–325.

[9] T. Eisenbarth, T. Unold, R. Caballero, C.A. Kaufmann, H.W. Schock, Interpretation of admittance, capacitance-voltage, and current-voltage signatures in Cu(In,Ga)Se_2 thin film solar cells, J. Appl. Phys. 107 (2010) 034509.

[10] T. Hölscher, T. Schneider, M. Maiberg, R. Scheer, Impact of air-light exposure on the electrical properties of Cu(In,Ga)Se_2 solar cells, Prog. Photovolt. Res. Appl. (2018) 1–8.

[11] M. Igalson, M. Edoff, Compensating donors in Cu(In,Ga)Se_2 absorbers of solar cells, Thin Solid Films 480-481 (2005) 322–326.

[12] A. Urbaniak, M. Igalson, N. Barreau, M. Tomassini, Capacitance spectroscopy of Cu(In,Ga)Se_2-based solar cells with a Pt back electrode, Thin Solid Films 574 (2015) 120–124.

[13] J.T. Heath, J.D. Cohen, W.N. Shafarman, Bulk and metastable defects in $CuIn_{1-x}Ga_xSe_2$ thin films using drive-level capacitance profiling, J. Appl. Phys. 95 (3) (2004) 1000–1010.

[14] R. Scheer, H.W. Schock, Chalcogenide Photovoltaics: Physics, Technologies and Thin Film Devices, Wiley-VCH, Weinheim, 2011.

[15] M. Maiberg, T. Hölscher, S. Zahedi-Azad, W. Fränzel, R. Scheer, Investigation of long lifetimes in Cu(In,Ga)Se_2 by time-resolved photoluminescence, Appl. Phys. Lett. 107 (2015) 122104.

[16] F. Werner, T. Bertram, J. Mengozzi, S. Siebentritt, What is the dopant concentration in polycrystalline thin-film Cu(In,Ga)Se_2? Thin Solid Films 633 (2017) 222–226.

[17] C.R. Crowell, The Richardson constant for thermionic emission in Schottky barrier diodes, Solid State Electron. 8 (1965) 395–399.

[18] T. Kobayashi, Z. Jehl Li Kao, T. Nakada, Temperature dependent current–voltage and admittance spectroscopy on heat-light soaking effects of Cu(In,Ga)Se_2 solar cells with ALD-Zn(O,S) and CBD-ZnS(O,OH) buffer layers, Sol. Energy Mater. Sol. Cells 143 (2015) 159–167.

[19] M. Richter, C. Schubbert, P. Eraerds, J. Parisi, I. Riedel, T. Dalibor, J. Palm, Comprehensive simulation model for Cu(In,Ga)$(Se,S)_2$ solar cells, Sol. En, Sol. Energy Mater. Sol. Cells 132 (2015) 162–171.

[20] H. Elanzeery, F. Babbe, M. Melchiorre, F. Werner, S. Siebentritt, High-performance low bandgap thin film solar cells for tandem applications, Prog. Photovolt. Res. Appl. (2018) 1–6.